NANO LETTERS

2009
Vol. 9, No. 4
1651-1658

Plasmon Coupling of Gold Nanorods at Short Distances and in Different Geometries

Alison M. Funston,*,† Carolina Novo,† Tim J. Davis,‡ and Paul Mulvaney†

School of Chemistry and Bio21 Institute, University of Melbourne, Parkville, Victoria, 3010, Australia, and CSIRO Materials Science and Engineering, Clayton South, Victoria, 3169, Australia

Received January 6, 2009; Revised Manuscript Received February 13, 2009

ABSTRACT

The experimentally determined scattering spectra of discrete, crystalline, gold nanorod dimers arranged side-to-side, end-to-end, at right angles in different orientations and also with longitudinal offsets are reported along with the electron micrographs of the individual dimers. The spectra exhibit both red- and blue-shifted surface plasmon resonances, consistent with the plasmon hybridization model. However, the plasmon coupling constant for gold dimers with less than a few nanometers separation between the particles does not obey the exponential dependence predicted by the Universal Plasmon Ruler equation. The experimentally determined spectra are compared with electrodynamic calculations and the interactions between the individual rod plasmons in different dimer orientations are elucidated.

The localized surface plasmon resonance (LSPR) of metallic nanoparticles is the result of the collective oscillation of conduction electrons within the particle upon interaction with light. The resonance energy of the LSPR is highly sensitive to the size and morphology of the particle.[1−3] The close approach (i.e., within 2.5 times the particle diameter) of two nanoparticles leads to interaction of their localized surface plasmon resonances. This interaction has been exploited in a number of applications, including surface-enhanced Raman spectroscopy (SERS) to allow the detection of single molecules,[4−8] the Universal Plasmon Ruler which has been used to measure the distance between two metal nanoparticles in biological systems,[9−12] and in optoelectronics where the near field coupling of nanoparticles spaced less than two diameters apart results in the transmission of light energy down a nanoparticle chain[13−17] or through an array.[18]

This near field interaction between nanoparticles is highly distance-dependent and has been described using an electromagnetic analogue of molecular orbital theory, the plasmon hybridization model, which highlights the asymmetry introduced by dimer formation.[19−22] When the electric field is oriented along the interparticle axis (for a given particle pair), the near fields couple in a manner analogous to a bonding interaction, resulting in a significant red shift of the plasmon.[9,10,23−28] When the polarization is oriented perpendicular to the interparticle axis on the other hand, their near fields couple in a nonbonding type of interaction and a very small blue shift of the plasmon band is observed.[10,26,27] For each of these arrangements the other possible interaction mode is a dark mode which cannot be excited by light due to the symmetry of the system. For spheres, the distance dependence of the coupling has been calculated using the plasmon hybridization model[20] and approximated as either a (d^{-3})[26] or exponential function for distances between 2 nm and 2.5 times the particle diameter, the coupling limit. The Universal Plasmon Ruler utilizes an exponential function to model the distance dependence of nanoparticles, enabling the measurement of distances between nanoparticles by measuring the plasmon resonance of two coupled particles.[9,10,26−28] However, until now, the degree of near field coupling at extremely small interparticle separation (less than 2 nm) has not been experimentally investigated.

Previous investigations of plasmon coupling have predominantly utilized electron beam lithography (EBL) to synthesize nanoparticle arrays, chains, and periodically repeating sets of nanoparticles organized as interacting pairs. However, the resolution limit of modern EBL fabrication is around 10 nm. While theoretical investigation of nanoparticle pairs less than 2 nm apart has been carried out,[29] experimental fabrication and investigation of such particle pairs have remained challenges. It has, in part, been overcome by the investigation of single-pair studies of nanoparticles complemented by electron microscopy images of the single pair[23,27,27] and the use of laser techniques to form a small gap between touching particles.[24] However, it is apparent in

* Corresponding author, afunston@unimelb.edu.au.
† The University of Melbourne.
‡ CSIRO.

10.1021/nl900034v CCC: $40.75
Published on Web 03/09/2009

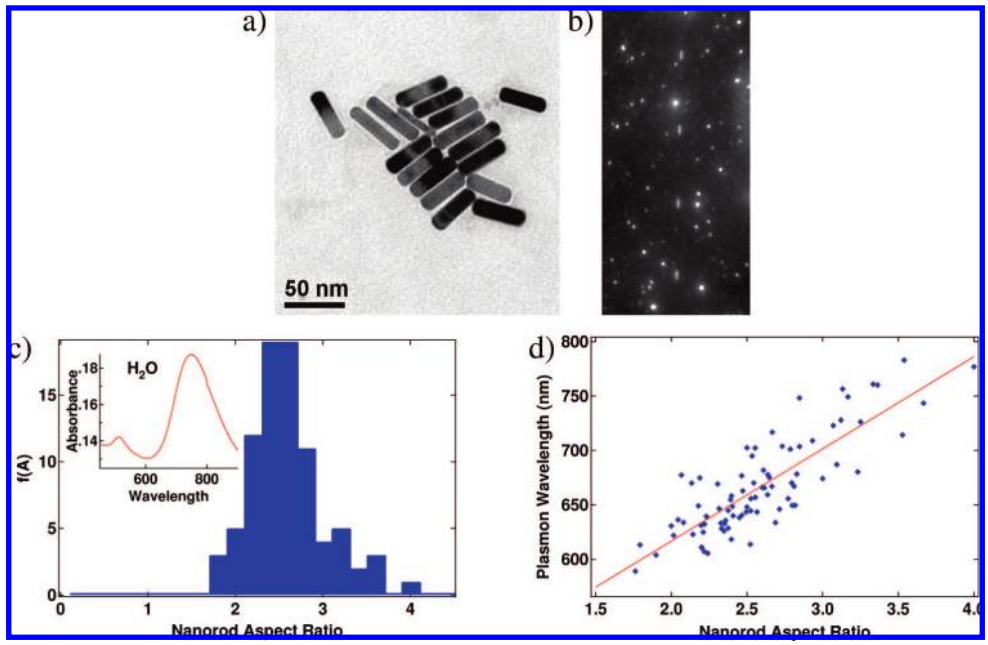

Figure 1. (a) TEM of gold rod sample, scale bar = 50 nm. (b) Dark-field image of markers etched in the substrate with gold rods. The gold rods scatter the incoming light and appear as the white spots in the image. (c) Frequency distribution of aspect ratios for gold nanorod sample. The inset shows the absorption spectrum of the ensemble in water. (d) Longitudinal plasmon band position as a function of rod aspect ratio. Each point is one rod for which the spectrum and SEM image were measured. The rods were dispersed on ITO-coated glass in air.

images of the fabricated particles that they contain not one but many crystalline domains and their perimeter is not well-defined, resulting in protrusions and inhomogeneities in the region of closest approach. In such cases it becomes difficult to determine whether the particles themselves are actually touching. Chemically synthesized nanoparticles on the other hand are discrete crystals of highly defined shape. The challenge for investigating these nanoparticles is the arrangement of the nanoparticles into well-defined configurations.

In this paper we report our investigation into the coupling between gold nanorods, with interparticle distances smaller than 2 nm. The shape anisotropy of nanorods leads to different possible orientations of the nanorods within the dimer, leading to different orientational modes of coupling. Coupling of the rod longitudinal modes when the dimer is arranged end-to-end or side-to-side leads to bonding and antibonding interactions. Hence upon coupling either an increase (side-to-side) or a decrease (end-to-end) in the resulting LSPR mode energy is expected. A similar picture exists for interaction of the rod transverse modes. We measure here for the first time the interactions between individual gold rod pairs in both side-to-side and end-to-end orientations at extremely close approach and compare their spectra to those determined by electrodynamic simulations. The nanorod anisotropy also gives rise to many other possible dimer geometries, including L-shaped and T-shaped dimers as well as dimers laterally and longitudinally displaced with respect to one another, and these are also measured at the single-dimer level and characterized in terms of the active coupled modes. All the orientations investigated are characterized by electron microscopy images of the single dimers and are measured experimentally for extremely close approaches. These data show that the design and assembly of plasmonic superstructures from nanocrystals will require incredibly precise tailoring of position and orientation.

The particles were chemically synthesized and are single crystals. The investigation was carried out utilizing the recently reported focused ion beam registration method, allowing correlation of the scanning electron microscopy (SEM) image of the particle pairs with their scattering spectrum.[30] The gold nanorods were synthesized by standard protocols.[31,32] The rods had aspect ratios that varied between 2 and 4. A representative transmission electron microscopy (TEM) image of the rods used along with the absorption spectrum of the rod ensemble and aspect-ratio frequency distribution are shown in parts a and c of Figure 1. The rods were dispersed on indium tin oxide (ITO) coated glass slides and markers were etched in the substrate using a focused ion beam (FIB) as displayed in Figure 1b. The etched markers were located and imaged, and the scattering spectra of the particles around the markers were collected using a dark field microscope. The microscope setup consisted of a 0.8−0.95 NA dry dark field condenser and Nikon Plan Fluor ELWD 40×/0.60 NA objective coupled to a MicroSpec 2150i and Pixis 1024B Acton thermoelectrically cooled charge-coupled device (CCD) (Princeton Instruments). It is important to note that the excitation light in this setup was not polarized. The SEM images of the same particles were also collected, allowing direct correlation of the size, shape, and arrangement of the dimers with the scattering spectrum.

Under the conditions used here, the SEM and scattering spectra of both single particles and particle pairs were collected. The dimers were formed largely fortuitously when the rods were spin-coated onto the ITO; the vast majority of

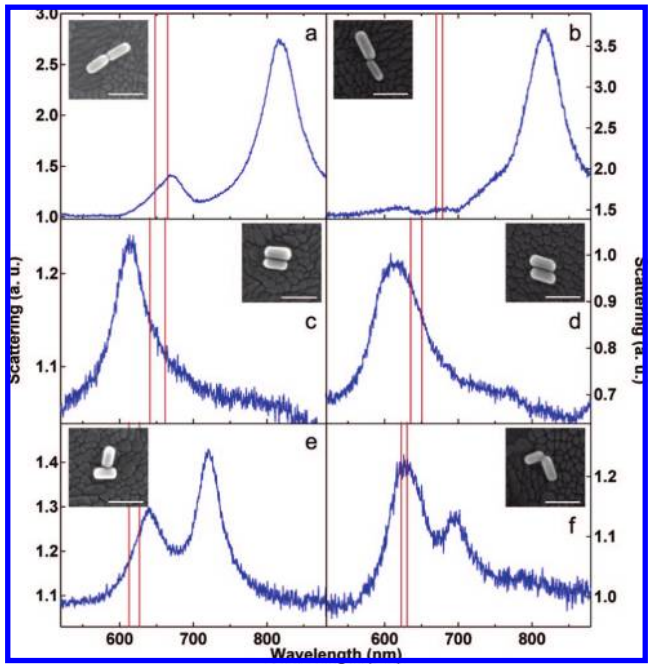

Figure 2. Scattering spectrum for two rods aligned (a and b) end-to-end, (c and d) side-to-side, (e) in a T configuration, and (f) in an L configuration, all on ITO and in air. Insets show the SEM images of the particles giving rise to each scattering spectrum. Scale bar = 100 nm.

rods in the samples existed as separated, single crystals. Investigations into the single particles will be reported in detail elsewhere,[33] although it is necessary to characterize the rod sample at a single-particle level for the following discussion. Figure 1d shows a plot of particle aspect ratio vs absorption wavelength for the longitudinal band of single rods. Consistent with earlier work,[34,35] the peak position of the longitudinal plasmon mode increases with an increase in the rod aspect ratio. The line in the figure is a line of best fit for this sample. There is scatter in the position of the plasmon band of around 80 nm for rods with a given aspect ratio.

The scattering spectra and SEM images of particle pairs arranged side-to-side, end-to-end, and at right angles were collected and a number of representative examples for each configuration are shown in Figure 2. All these particle pairs are arranged as close as possible to one another; from the SEM image we estimate this spacing is <1 nm. This is an upper limit as the resolution of the SEM is 1 nm. The surfactant molecules coating the gold rods are 1−1.5 nm long, so complete interdigitation would also lead to a separation of order 1 nm. Within these dimers, the two particles are interacting; however, the individual resonances of the two rods in the fully decoupled limit vary slightly due to small differences in aspect ratio. The individual rods shown in Figure 2 have aspect ratios varying between 2 and 2.7. From the line of best fit in Figure 1d, their individual plasmon resonances are expected to vary between 612 and 679 nm and the vertical lines in each part of Figure 2 represent the expected position of the plasmon bands for noninteracting single particles of identical dimensions to the rods in that specific dimer. The exact plasmon shift occurring as a result of the plasmon coupling in the dimers depends on the aspect ratio of each rod within the dimer; as a result we report here either the lower limit or a range for this shift.

Rods Aligned End-to-End. For the rods interacting end-to-end shown in Figure parts a and b of 2, the scattering spectra are dominated by an extremely intense peak which is red-shifted by more than 135 nm to >800 nm (for the two dimers shown $\lambda_{max} = 816$ nm) when compared to the expected longitudinal plasmon band of the individual rods in these two dimers, which range from 648 to 679 nm. The red shift is due to the attractive coupling of the rod longitudinal plasmon modes, as has previously been observed for spherical nanoparticles. This trend is consistent with that observed in ensemble measurements during the consecutive linear alignment of rods using linkers which have been shown to selectively bond to the ends of gold rods.[36−38] The fractional red shift, $\Delta\lambda/\lambda_o$ of the rods shown in Figure 2a is 0.24.

Discrete dipole approximation (DDA) electrodynamic simulations have been shown to be suitable for the calculation of scattering spectra of small gold particles[39] and particle pairs,[27] and this method has recently been reviewed and compared with alternative methods.[22] We utilized the program DDSCAT for the calculations, implemented and made freely available by Draine and Flatau.[40] Parameters used in the calculations are outlined in the Supporting Information. The DDA simulations for two rods with aspect ratio 2.0, rod length 60 nm, and hemispherically capped ends in an end-to-end geometry are consistent with earlier calculations[21,41] (Figure 3a). Incident light polarized parallel to the interparticle axis results in the selective excitation of the rod longitudinal modes. The longitudinal plasmon modes of the two rods interact via an attractive coupling with the opposite poles of the induced dipoles arranged in an alternating fashion. The induced surface-charge density of this coupled mode in longitudinally aligned rods is shown in Figure 4. The interaction results in a lowering of the energy of this resonance (relative to the longitudinal mode of a noninteracting rod), and as a consequence a red shift of the resonance is observed. When the light is polarized perpendicular to the interparticle axis, the transverse modes of the rods are excited; however, no appreciable shift is observed due to the weak coupling in this case. The polarization-averaged spectra are dominated by the interacting longitudinal plasmon mode due to its much higher polarizability. When the DDA data are scaled for the rod length, D, and plotted against the relative plasmon shift according to the Plasmon Ruler model (eq 1),[9,10,27,28] (see inset to Figure 3a) the distance dependence is approximately exponential for separations greater than 5 nm with $A = 0.12 \pm 0.01$ and $\tau = 0.26 \pm 0.04$.

$$\frac{\Delta\lambda}{\lambda_o} \approx Ae^{-(s/D)/\tau} \quad (1)$$

Figure 5 shows the experimentally determined and DDA calculated fractional shifts with interparticle distances 5 nm and less. Including DDA calculations for interparticle separations smaller than 5 nm in the determination of the plasmon

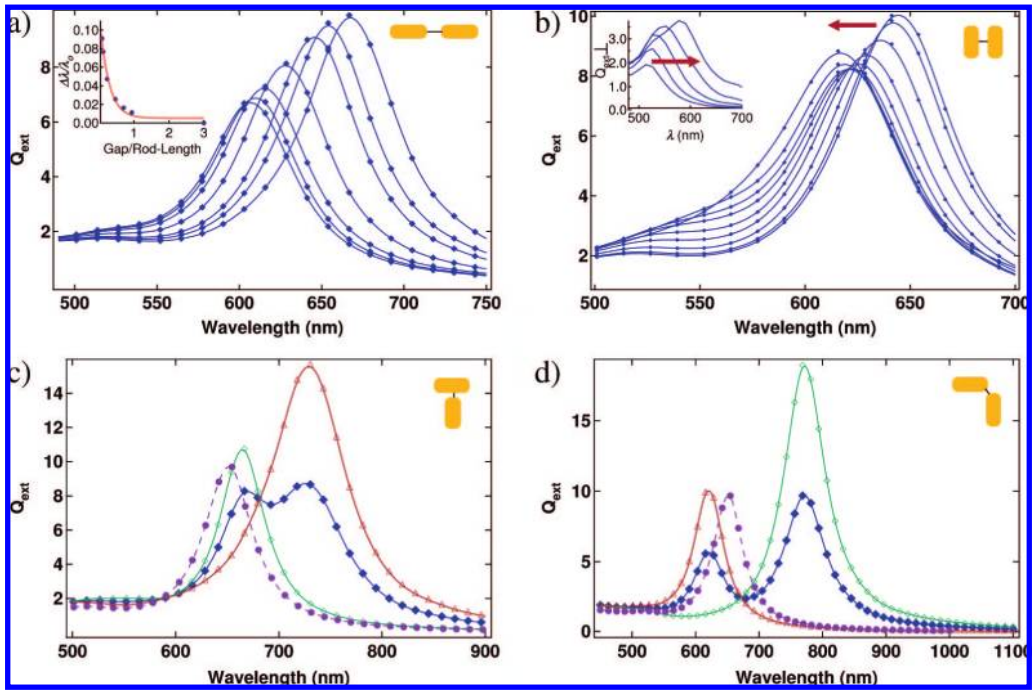

Figure 3. (a) Polarization averaged extinction of a pair of gold hemispherically capped rods with aspect ratio 2.0 interacting end-to-end as a function of interparticle separations 56.5, 42.4, 28.2, 14.1, 7.1, 5.3, and 3.5 nm with smaller separations more red shifted. Inset: Fractional shift of the longitudinal plasmon band as a function of interparticle distance scaled for rod length. The point at Gap/Rod-Length = 3 represents the plasmon resonance of a fully decoupled rod with the same dimensions as those in the dimer. (b) Polarization averaged extinction of a pair of hemispherically capped gold rods with aspect ratio 2.5 interacting side-to-side as a function of interparticle separation from 42.9, 12.9, 5.7, 2.9, and 1.4 nm with smaller separations more blue shifted. Inset: Extinction for polarization parallel to interparticle axis at d = 42.9, 12.9, 5.7, 2.9, and 1.4 nm, smaller separations more red shifted. (c) Extinction spectra of a pair of gold hemispherically capped rods interacting in a T geometry where the polarization is parallel to the interparticle axis (open triangles), perpendicular to the interparticle axis (open diamonds), and polarization averaged (solid diamonds), the calculated spectrum for a single rod is included for reference (closed circles). (d) Extinction spectra of a pair of gold hemispherically capped rods interacting in an L geometry with polarization parallel to the interparticle axis (open diamonds), perpendicular to the interparticle axis (open triangles), and polarization averaged (solid diamonds), the calculated spectrum for a single rod is included for reference (closed circles). For all calculations, rods are immersed in a homogeneous medium with a refractive index of 1.56[42] and the interparticle axis is defined by the black line connecting the nanorods in the schematic figures of the rod geometry.

decay led to poor fits to an exponential function. The accuracy of the DDA calculations at close approaches (i.e., for $s/D < 0.09$) is unclear due to the discretization of the rods as an array of point dipoles with an interdipole spacing of the order of 1−2 nm as used here. Experimentally, for the rods shown in Figure 2a, $s/D = 0.015$ and $\Delta\lambda/\lambda_o = 0.24$ while for those in Figure 2b, $s/D = 0.013$ and $\Delta\lambda/\lambda_o = 0.21$. DDA simulations of two rods with aspect ratio 2.4 and separation s = 1.43 nm give $s/D = 0.020$ and $\Delta\lambda/\lambda_o = 0.2$, and these values are consistent with those obtained experimentally, particularly as the experimental rod separation cannot be determined with greater accuracy than 1 nm. It may be concluded that the exponential decay of the plasmon interaction serves only as an empirical approximation for the interaction and is valid only if the ratio of interparticle separation (s) to rod length (or diameter in the case of spheres) (D) is greater than 5.3 nm/60 nm = 0.09 according to our DDA and experimental results.

Additional modes at higher energies are also obvious in the spectra of the single particles in Figure 2a. A similar feature, attributed to hybridization of the individual plasmon modes at small interparticle separations has been predicted theoretically,[20,29,45] and was observed following laser-induced separation of previously touching spheres which resulted in

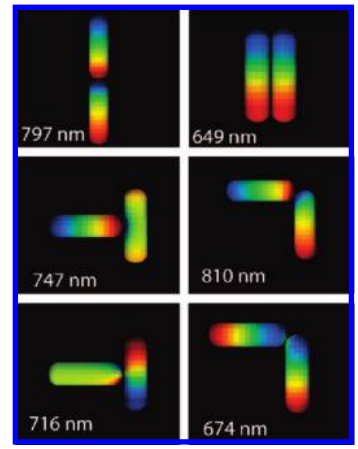

Figure 4. Surface charge density of interacting cylindrical, spherically capped gold nanorods placed 1.5 nm apart and with dimensions 78 nm × 24 nm, calculated using the electrostatic approximation[43,44] and where blue represents one charge (for example −ve) and the red the opposite charge (+ve) of the dipole. The plasmon resonance for a single rod of these dimensions calculated using this method is 707 nm. The wavelength given is the resonance wavelength for the coupled plasmon mode. The general trends in the resonance wavelengths are identical to those calculated using DDA.

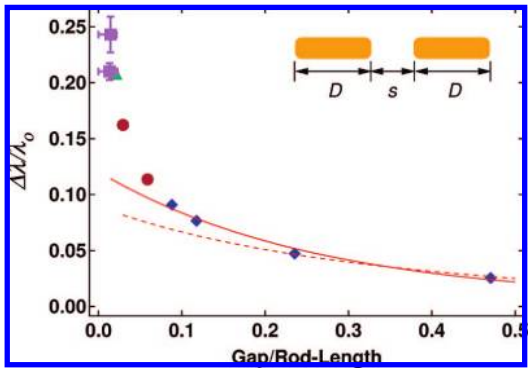

Figure 5. Fractional shift of longitudinal plasmon band of spherically capped gold nanorods as a function of interparticle distance scaled for rod length determined experimentally (purple squares) and by DDA simulations for rods with aspect ratio 2.0 where $s/D > 0.09$ (blue diamonds). The red line is an exponential fit to these data and the dashed line is the $1/d^3$ fit, $s/D < 0.05$ with interdipole spacing 1.76 nm (red circles) and $s/D = 0.020$ with aspect ratio 2.4 and interdipole spacing = 1.43 nm (green triangle). Medium $\eta = 1.56$.

$s/D = 0.03$.[24] The presence of an additional resonance mode has also been predicted by DDA simulations for the end-to-end longitudinal plasmon coupling of rods with different aspect ratios due to symmetry breaking, resulting in the previously optically inactive transition at higher energy with net dipole = 0 gaining a nonzero dipole.[21] However, the two rods interacting in Figure 2a have similar dimensions, and rod dimers with lower symmetry do not display a similar, higher energy mode (see Figure 2b). From these considerations we conclude it is most likely that the additional high-energy peak is due to hybridization of the plasmon modes at the small interparticle separation in this rod pair.

Rods Aligned Side-by-Side. In contrast to the case for rods aligned end-to-end, the spectra of rod dimers aligned in a side-by-side configuration display a single peak with scattering intensity comparable to that for a single rod, at a wavelength that is blue-shifted by 21−48 nm compared to single rods (to λ_{max} 614 nm). In this arrangement, when the polarization is parallel to the interparticle distance, the low intensity transverse plasmon modes interact attractively and these undergo a red shift as the particles approach. This is obvious in the DDA calculations (see inset to Figure 3b). However, the polarization-averaged spectra are dominated by the longitudinal plasmons of the rods which interact repulsively, leading to a slight blue shift overall and the red shift of the transverse bands is washed out. The surface charge density associated with this mode is shown in Figure 4 and is in accordance with the predictions from the plasmon hybridization model. These results are consistent both with ensemble data where the nanorods align side-to-side[21] and with previously reported DDA simulations.[21,41]

Rods Arranged In T and L Geometries. Rod dimers in which the rods are arranged at right angles introduces the possibility of coupling between longitudinal and transverse modes. Two rods arranged in T- and L-shaped configurations along with their scattering spectra are shown in parts e and f of Figure 2, and the extinction calculated via DDA for these two configurations and at different polarizations are shown in parts c and d of Figure 3. Particles in these configurations have the potential to form the basis of right-angle and T-junction structures in plasmonic circuits. For these particle pairs, intuitively it may be predicted that the transverse mode of one rod interacts with the longitudinal mode of the other rod.

Two well-separated plasmon modes are present in the scattering spectra of rods in an "L" configuration. These modes are reproduced in the DDA calculations performed here, which differ somewhat from those reported previously for two rods interacting at right angles.[21] Polarization of the incoming radiation along the interparticle axis leads to excitation of a lower-energy, attractive mode in which the two longitudinal plasmons are oscillating in phase with one another, resulting in dipoles with opposing signs where the rods approach (see Figure 4). When the polarization is perpendicular to the interparticle axis, the longitudinal plasmon bands of the two rods oscillate symmetrically out of phase and the dipoles interact repulsively. It is interesting to note that for the L configuration, the coupled modes are all due to interactions between the longitudinal plasmon modes of the rods and not longitudinal-transverse coupling.

Conversely, for the rods in a T-configuration, interactions do occur between the longitudinal and transverse modes of the rods. Excitation with light polarized along the interparticle axis results in the excitation of the longitudinal mode of the rod forming the stem of the "T". This excitation interacts with a mode of the opposing sign in the center of the other rod, lowering its energy slightly. Conversely, excitation with light polarized perpendicular to the interparticle axis results in the excitation of the rod forming the top rod of the "T", which is able to interact to a small degree with a dipole-like mode of the perpendicular rod (see Figure 4). It is possible these plasmon interactions in the "T" dimer are predominantly dipole−induced dipole interactions in character. For this arrangement, the energy difference between the two modes is calculated to be quite small, although this is not reflected in the experimental data.

Offset Rods. The experimental scattering spectra for a number of pairs of rods interacting side-to-side but longitudinally offset with respect to one another are shown in Figure 6. DDA calculations for this geometry as a function of rod offset as well as the corresponding geometry and offsets for rods interacting end-to-end are shown in Figure S1 of Supporting Information. For the latter, DDA results show that as one rod is displaced further and further from the axis of the other, the coupling between the two rods weakens as expected. This is observed as a blue shift of the spectrum with increasing offset compared to the highly coupled, fully aligned rods and a concomitant decrease in the extinction.

DDA results for rods interacting side-to-side but longitudinally shifted with respect to one another are quite different from those for the end-to-end geometry. The peak positions as a function of rod offset are given in Figure 7. Two distinct effects are important. For both zero and small longitudinal shifts, the repulsively interacting longitudinal modes dominate the spectra and a weakening of the intensity as the

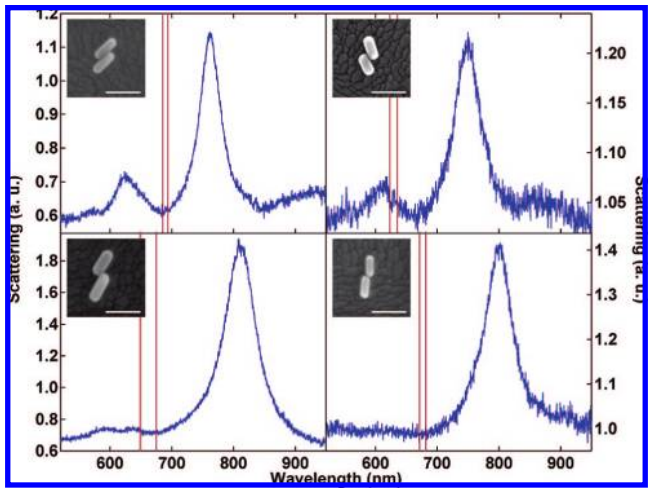

Figure 6. Scattering spectra for two rods aligned side-to-side on ITO and in air with various lateral offsets. Insets show the SEM images of the particles giving rise to each scattering spectrum. Scale bar = 100 nm.

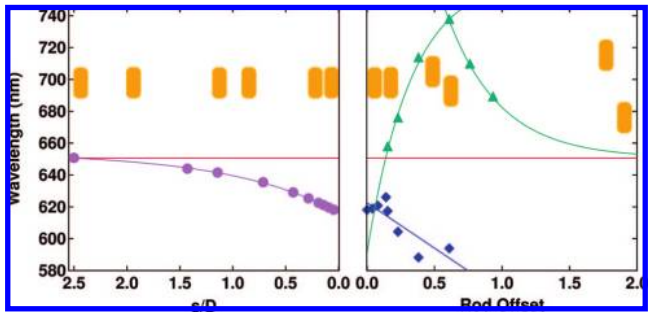

Figure 7. Wavelength of peak maximum for spherically capped gold rods interacting side-by-side as a function of transverse separation and lateral separation as determined by DDA calculations. All modes are due to interaction of the longitudinal modes of the rods. The lines are exponential fits to the data intended as a rough guide to the eye. Medium $\eta = 1.56$.

center-to-center distance of the rods increases is observed. However, even at small offsets (23%), another lower-energy mode grows in. This is a result of the lifting of symmetry within the system. The attractive coupling between the longitudinal modes becomes allowed as the dipole moment for this transition becomes nonzero as the rods are offset. At an offset of 38%, the attractively and repulsively coupled longitudinal modes give rise to two well-separated peaks in the spectrum; the repulsive longitudinal coupling has decreased considerably as the tips of the rods are further from one another.

A further increase of the offset between the rods causes the opposite ends of the two rods to approach one another, and the repulsive coupling between the longitudinal modes then becomes attractive due to the opposing signs of the field at the opposite ends of the rods. This gives rise to a lowering in energy for this mode as reflected by the strongly red-shifted resonance. As the separation increases and the fields at the opposite ends of the rods approach one another, this resonance becomes more and more red shifted and intense up to an offset of 61% where maximum coupling occurs.

As the rods move further apart again (>61% center-to-center separation), attractive coupling of the longitudinal modes again decreases as the fields move away from one another and the coupling decreases. When the radiation is polarized parallel to the interparticle axis and the transverse modes are excited, a similar effect is observed but in reverse; this is not obvious in the polarization-averaged spectra. The experimental data (Figure 6) are consistent with the DDA results. At smaller rod-to-rod displacements of about 20−50%, two bands are observed in the experimental scattering spectra. However, as the ends of the rods approach one another, the low-energy mode experiences a stronger coupling and red shifts and increases in intensity.

These experimental results highlight a number of important aspects about the potential use of plasmon coupling as a molecular ruler and for the transport of electromagnetic energy.

In the dipole approximation, the near field of a plasmon dipole mode is well-known to decay as $1/d^3$, where d is the distance from the particle. Analogously, it has been shown that dipole−dipole coupling (within the dipole approximation) also decays as $1/d^3$;[26] in this case d is the center-to-center distance between the two coupled particles. However, as the particles approach to very small separations, the finite particle size along with interactions of the dipole mode on one particle with higher modes on its pair become important and the dipole coupling model becomes invalid. The plasmon ruler equation[10] is based upon an exponential function. This is primarily due to the observation that calculated data sets which included smaller interparticle distances, $s/D = 0.1$, were described better at smaller separations by an exponential function compared to the dipole coupling model.

Both functions, that is, exponential and d^{-3}, have been successfully used to model the plasmon resonance shifts observed experimentally for larger interparticle separations.[26−28] However, we find here that neither function is able to successfully model the experimentally observed distance dependence of coupled nanoparticles over the full interaction range, with significant deviations occurring for both these models at small interparticle distances where the energy of the longitudinally coupled plasmon mode red shifts much more rapidly than that predicted by either model. The exponential model significantly underestimates the shift in the plasmon energy due to coupling at very small distances, $s/D < 0.09$. As a result of this, it is necessary to use more sophisticated calculations to completely and correctly describe the plasmon shift observed at small interparticle separations, such as the plasmon hybridization method[19,20] and extended multipole methods. These methods take into account the hybridization of the dipole mode of one particle with higher-order multipoles on its pair, resulting in additional, higher-order terms to the plasmon coupling at small distances. Calculations performed using the plasmon hybridization method for two 10 nm radius spheres with polarization of the electric field parallel to the interparticle axis[20] replicates the large red shift experimentally observed here at small interparticle distances.

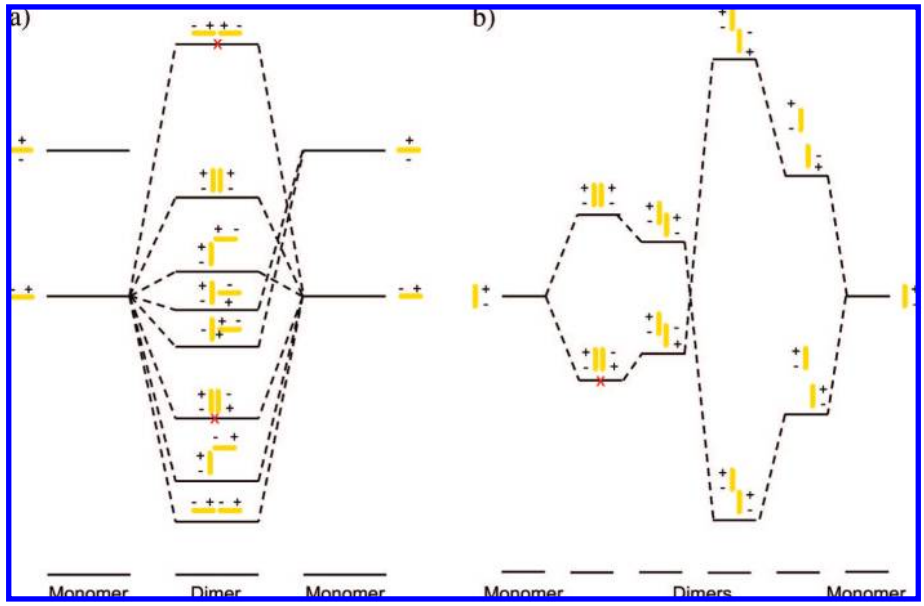

Figure 8. Plasmon hybridization schemes for (a) rod dimers in different geometric arrangements and (b) rods initially arranged side-to-side and then increasingly longitudinally offset as a function of the center-to-center offset.

While the use of rods would improve accuracy for measurements of distance using the Plasmon Ruler due to their higher signal and larger shift, their intrinsic advantage, the particle asymmetry, actually precludes their use in experiments designed to use plasmon coupling as a measure of distance. This is a result of the dependence of the coupling on the geometrical arrangement of the rods, which is extremely difficult to control. Because of the unpredictability of the rod arrangement, the interaction between spheres is more reliable as a method for measuring distances.

The asymmetry of the rods leads to a number of different trajectories for the approach of two rods into a common alignment. This is highlighted by the results from the DDA calculations in Figure 7, where two rods approach one another differently to align side-to-side. For direct approach of the rods with no longitudinal displacement (left panel), the longitudinal coupling results in a gradual blue shift of the plasmon relative to an uncoupled rod, the energy of which is given by the horizontal line at 651 nm. The right panel shows the rods approaching via a longitudinal translation of the rods. For this trajectory, the symmetry of the system is lowered compared to the direct side-to-side approach and this is reflected in the higher number of modes apparent in the spectrum as the particles approach. Despite the different trajectories for the rod alignment, the end result is ultimately the same.

For dimers incorporating rods, a large number of possibilities for the arrangement of the individual rods dimers exist, and these display very different plasmon coupling modes and degrees of coupling. In Figure 8a we have extended the plasmon hybridization diagrams for rods to include dimers interacting at right angles. For clarity, transverse−transverse interactions have been omitted as these effectively mirror the longitudinal−longitudinal interactions. The relative energetics shown are qualitative. In contrast to linearly aligned rods, for which symmetry considerations result in one of the modes being dark (the higher energy mode for rods aligned end-to-end and the lower energy mode for rods aligned side-to-side), lifting of this symmetry results in all modes being optically active. It is clear that hybridization between two longitudinal modes leads to greater splitting, although the degree of splitting is geometry dependent and rods aligned with their tips approaching display greater splitting. In turn, geometries in which the coupling is between longitudinal and transverse modes experience less splitting.

These experiments highlight important differences between coupling for practical waveguiding applications. While both the "L" and "T" geometries are models for T junctions in optical circuits, for these geometries to act as T junctions strong coupling between the two rods must occur. From the results here, it is obvious that coupling within the T geometry is not particularly strong as it is a longitudinal−transverse interaction and excitation of the longitudinal mode of either rod does not lead to significant transfer of this energy into the other rod. The L geometry, on the other hand, involves strong coupling between two longitudinal modes with transmission of the plasmon resonance throughout the full structure.

The plasmon hybridization diagram for two rods aligned side-to-side and then sequentially longitudinally offset with respect to one another is shown in Figure 8b. Initially, for the fully aligned rods, hybridization results in the formation of two energy levels. The longitudinal plasmon modes of the rods interact symmetrically in the higher-energy, repulsive mode while the lower-energy mode is dark. A small longitudinal shift of the rods reduces the symmetry present in the previously dark state, resulting in it becoming allowed. The splitting however is slightly weaker. A further longitudinal shift results in an energetic cross-over of states, with the symmetric mode becoming attractive due to the proximity of the oppositely charged rod tips to one another. Further

displacement lowers the coupling energy for both modes significantly.

In summary, we have established the viability and versatility of one-dimensional rod structures for the tuning of the LSPR in plasmonic structures. This coupling may be controlled through nanoparticle separation, angle, and interaction geometry. We have elucidated new hybridization interactions which are introduced due to the different possible interaction geometries of the rods, enabling one to engineer surface plasmon resonances. The form of the distance dependence of the plasmon coupling between nanoparticles has been extended to include small interparticle distances. These results show that the approximation of the coupling distance dependence according to the dipole−dipole approximation or as an exponential does not hold for nanoparticles separated by only a few nanometres or less and that the plasmon ruler equation, therefore, is not valid for *s*/*D* ratios less than 0.09.

These results highlight the importance of orientation on the coupling of anisotropic nanoparticles such as rods. Small changes in the rod orientation lead to relatively large changes in the plasmon interaction, particularly at close approach.

Acknowledgment. This work was supported through ARC DP Grant 0451651 and FF Grant 0561486. The authors thank Sergey Rubanov for assistance with FIB/SEM. C.N. thanks the University of Melbourne for MIRS and MIFRS postgraduate scholarships.

Supporting Information Available: DDA calculation details and figure showing polarization averaged extinction of a pair of spherically capped cylindrical gold rods. This material is available free of charge via the Internet at http://pubs.acs.org.

References

(1) Kelly, K. L.; Coronado, E.; Zhao, L. L.; Schatz, G. C. *J. Phys. Chem. B* **2003**, *107*, 668–677.
(2) Sihvola, A. *J. Nanomaterials* **2007**, Special Issue 1, 45090.
(3) Prescott, S. W.; Mulvaney, P. *J. Appl. Phys.* **2006**, *99*, 123504. Prescott, S. W.; Mulvaney, P. *J. Appl. Phys.* **2008**, *103*, 119901.
(4) Kneipp, K.; Wang, Y.; Kneipp, H.; Perelman, L. T.; Itzkan, I.; Dasari, R. R.; Feld, M. S. *Phys. Rev. Lett.* **1997**, *78*, 1667–1670.
(5) Kneipp, K.; Kneipp, H.; Kneipp, J. *Acc. Chem. Res.* **2006**, *39*, 443–450.
(6) Nie, S.; Emory, S. R. *Science* **1997**, *275*, 1102–1106.
(7) Michaels, A. M.; Jiang, J.; Brus, L. *J. Phys. Chem. B* **2000**, *104*, 11965–11971.
(8) Camden, J. P.; Dieringer, J. A.; Wang, Y.; Masiello, D. J.; Marks, L. D.; Schatz, G. C.; Duyne, R. P. V. *J. Am. Chem. Soc.* **2008**, *130*, 12616–12617.
(9) Reinhard, B. M.; Siu, M.; Agarwal, H.; Alivisatos, A. P.; Liphardt, J. *Nano Lett.* **2005**, *5*, 2246–2252.
(10) Jain, P. K.; Huang, W.; El-Sayed, M. A. *Nano Lett.* **2007**, *7*, 2080–2088.
(11) Sönnichsen, C.; Reinhard, B. M.; Liphardt, J.; Alivisatos, A. P. *Nat. Biotechnol.* **2005**, *23*, 741–745.
(12) Reinhard, B. M.; Sheikholeslami, S.; Mastroianni, A.; Alivisatos, A. P.; Liphardt, J. *Proc. Natl. Acad. Sci. U.S.A.* **2007**, *104*, 2667–2672.
(13) Brongersma, M. L.; Hartman, J. W.; Atwater, H. A. *Phys. Rev. B* **2000**, *62*, R16 356–359.
(14) Maier, S. A.; Brongersma, M. L.; Kik, P. G.; Meltzer, S.; Requicha, A. A. G.; Atwater, H. A. *Adv. Mater.* **2001**, *13*, 1501–1505.
(15) Maier, S. A.; Kik, P. G.; Atwater, H. A.; Meltzer, S.; Harel, E.; Koel, B. E.; Requicha, A. A. G. *Nat. Mater.* **2003**, *2*, 229–232.
(16) Krenn, J. R.; Dereux, A.; Weeber, J. C.; Bourillot, E.; Lacroute, Y.; Goudonnet, J. P.; Schider, G.; Gotschy, W.; Leitner, A.; Aussenegg, F. R. *Phys. Rev. Lett.* **1999**, *82*, 2590–2593.
(17) Quinten, M.; Leitner, A.; Krenn, J. R.; Aussenegg, F. R. *Opt. Lett.* **1998**, *23*, 1331–1333.
(18) Maier, S. A.; Friedman, M. D.; Barclay, P. E.; Painter, O. *Appl. Phys. Lett.* **2005**, *86*, 071103.
(19) Prodan, E.; Radloff, C.; Halas, N. J.; Nordlander, P. *Science* **2003**, *302*, 419–422.
(20) Nordlander, P.; Oubre, C.; Prodan, E.; Li, K.; Stockman, M. I. *Nano Lett.* **2004**, *4*, 899–903.
(21) Jain, P. K.; Eustis, S.; El-Sayed, M. A. *J. Phys. Chem. B* **2006**, *110*, 18243–18253.
(22) Myroshnychenko, V.; Rodriguez-Fernandez, J.; Pastoriza-Santos, I.; Funston, A. M.; Novo, C.; Mulvaney, P.; Liz-Marzán, L. M.; García de Abajo, F. J. *Chem. Soc. Rev.* **2008**, *37*, 1792–1805.
(23) Tamaru, H.; Kuwata, H.; Miyazaki, H. T.; Miyano, K. *Appl. Phys. Lett.* **2002**, *80*, 1826–1828.
(24) Atay, T.; Song, J.-H.; Nurmikko, A. V. *Nano Lett.* **2004**, *4*, 1627–1631.
(25) Prikulis, J.; Svedberg, F.; Käll, M.; Enger, J.; Ramser, K.; Goksör, M.; Hanstorp, D. *Nano Lett.* **2004**, *4*, 115–118.
(26) Rechberger, W.; Hohenau, A.; Leitner, A.; Krenn, J. R.; Lamprecht, B.; Aussenegg, F. R. *Opt. Commun.* **2003**, *220*, 137–141.
(27) Gunnarsson, L.; Rindzevicius, T.; Prikulis, J.; Kasemo, B.; Käll, M.; Zou, S.; Schatz, G. C. *J. Phys. Chem. B* **2005**, *109*, 1079–1087.
(28) Su, K.-H.; Wei, Q.-H.; Zhang, X.; Mock, J. J.; Smith, D. R.; Schultz, S. *Nano Lett.* **2003**, *3*, 1087–1090.
(29) Romero, I.; Aizpurua, J.; Bryant, G. W.; Abajo, F. J. G. d. *Opt. Exp.* **2006**, *14*, 9988–9999.
(30) Novo, C.; Funston, A. M.; Pastoriza-Santos, I.; Liz-Marzán, L. L.; Mulvaney, P. *Angew. Chem., Int. Ed.* **2007**, *46*, 3517–3520.
(31) Nikoobakht, B.; El-Sayed, M. A. *Chem. Mater.* **2003**, *15*, 1957–1962.
(32) Pérez-Juste, J.; Liz-Marzán, L.; Carnie, S.; Chan, D. Y. C.; Mulvaney, P. *Adv. Funct. Mater.* **2004**, *14*, 571–579.
(33) Novo, C.; Funston, A. M.; Rodriguez-Fernandez, J.; Liz-Marzán, L. M.; Mulvaney, P. Manuscript in preparation, 2008.
(34) Yu, Y.-Y.; Chang, S.-S.; Lee, C.-L.; Wang, C. R. C. *J. Phys. Chem. B* **1997**, *101*, 6661–6664.
(35) Pérez-Juste, J.; Pastoriza-Santos, I.; Liz-Marzán, L. M.; Mulvaney, P. *Coord. Chem. Rev.* **2005**, *249*, 1870–1901.
(36) Thomas, K. G.; Barazzouk, S.; Ipe, B. I.; Joseph, S. T. S.; Kamat, P. V. *J. Phys. Chem. B* **2004**, *108*, 13066–13068.
(37) Joseph, S. T. S.; Ipe, B. I.; Pramod, P.; Thomas, K. G. *J. Phys. Chem. B* **2006**, *110*, 150–157.
(38) Pramod, P.; Thomas, K. G. *Adv. Mater.* **2008**, *20*, 4300.
(39) Yang, W.-H.; Schatz, G. C.; Duyne, R. P. V. *J. Chem. Phys.* **1995**, *103*, 869–875.
(40) Draine, B. T.; Flatau, P. J. *DDSCAT*.
(41) Jain, P. K.; El-Sayed, M. A. *J. Phys. Chem. C* **2008**, *112*, 4954–4960.
(42) Novo, C.; Funston, A. M.; Pastoriza-Santos, I.; Liz-Marzán, L. M.; Mulvaney, P. *J. Phys. Chem. C* **2008**, *112*, 3–7.
(43) Mayergoyz, I. D.; Fredkin, D. R.; Zhang, Z. *Phys. Rev. B* **2005**, *72*, 155412.
(44) Mayergoyz, I. D.; Zhang, Z.; Miano, G. *Phys. Rev. Lett.* **2007**, *98*, 147401.
(45) Kottmann, J. P.; Martin, O. J. F. *Opt. Lett.* **2001**, *26*, 1096–1098.

NL900034V